

Article

Cholesteric Liquid Crystal Photonic Hydrogel Films Immobilized with Urease Used for the Detection of Hg²⁺

Jie Liu †, Wenjun Tai †, Deliang Wang, Jie Su and Li Yu *

Key Laboratory of Colloid and Interface Chemistry, Shandong University, Ministry of Education, Jinan 250100, China; liujie7613@tju.edu.cn (J.L.); 202012292@mail.sdu.edu.cn (W.T.); dlwang1991@zju.edu.cn (D.W.); sjtj90@sdu.edu.cn (J.S.)

* Correspondence: ylmlt@sdu.edu.cn; Tel.: +86-531-88364807

† These authors contributed equally to this work.

Abstract: Mercury ion is one of the most widespread heavy metal contaminants which can accumulate in the body through multiple channels, posing a detrimental impact on human health. We demonstrate a simple and low-cost method for the detection of Hg²⁺ assisted by a cholesteric liquid crystal photonic hydrogel (polyacrylic acid (PAA)) film with immobilized urease (CLC-PAA_{urease} film). In the absence of Hg²⁺, a significant change in color and an obvious red shift in the reflected light wavelength of the prepared film were observed, since urease can hydrolyze urea to produce NH₃, resulting in an increasing pH value of the microenvironment of CLC-PAA_{urease} film. Hg²⁺ can inhibit the activity of urease so that the color change of the film is not obvious, corresponding to a relatively small variation of the reflected light wavelength. Therefore, Hg²⁺ can be quantitatively detected by measuring the displacement of the reflected light wavelength of the film. The detection limit of Hg²⁺ is about 10 nM. This approach has a good application prospect in the monitoring of heavy metal ions in environmental water resources.

Keywords: cholesteric liquid crystal; photonic hydrogel film; polyacrylic acid; mercury ion; detection



Citation: Liu, J.; Tai, W.; Wang, D.; Su, J.; Yu, L. Cholesteric Liquid Crystal Photonic Hydrogel Films Immobilized with Urease Used for the Detection of Hg²⁺. *Chemosensors* **2022**, *10*, 140. <https://doi.org/10.3390/chemosensors10040140>

Academic Editor: Francesco Dell'Olio

Received: 15 February 2022

Accepted: 6 April 2022

Published: 8 April 2022

Publisher's Note: MDPI stays neutral with regard to jurisdictional claims in published maps and institutional affiliations.



Copyright: © 2022 by the authors. Licensee MDPI, Basel, Switzerland. This article is an open access article distributed under the terms and conditions of the Creative Commons Attribution (CC BY) license (<https://creativecommons.org/licenses/by/4.0/>).

1. Introduction

With the development of modern industry, heavy metal ion pollution has become a great danger to the environment and the human body [1]. Hg²⁺ is a highly toxic heavy metal ion. It accumulates in large quantities in rivers and aquatic organisms and enters the human body through the food chain and other channels [2,3]. Due to its non-biodegradable and accumulative nature, Hg²⁺ cannot be excreted from the body. It can cause varying degrees of damage to the human respiratory, digestive and nervous systems, even in very small amounts [4,5]. Hg²⁺ in the environment combines with various ligands to form complexes and is converted to methylmercury and dimethylmercury by the action of microorganisms, which is known as the biomethylation of mercury [6–8]. Because methylmercury is readily soluble in lipids and the carbon–mercury bonds in its molecular structure are not readily broken down, it is readily absorbed by the body, excreted slowly and has a higher toxicity profile. Therefore, the detection of Hg²⁺ has attracted much attention [9].

A variety of Hg²⁺ detection methods have been established such as atomic absorption spectrometry [10–12], inductively coupled plasma mass spectrometry (ICP-MS) [13–15], electrochemical methods [16–18] and fluorescence spectrometry [19–21]. Although these assays of Hg²⁺ have high sensitivity, they usually require large, expensive instruments, specialized technicians and time-consuming operations [22]. In addition, some existing Hg²⁺ detection methods even require molecular markers, which are not conducive to the rapid and continuous monitoring of Hg²⁺ in actual environments. Therefore, it is an urgent task to develop a new strategy to detect Hg²⁺ with some advantages such as low cost and simple operation.

The photonic crystal (PC) has broad application prospects in constructing the optical sensor, which can be attributed to its excellent optical properties [23–25]. The cholesteric liquid crystal (CLC) is a periodic arrangement of twisted layers of parallel, aligned rod-like molecules or nano-objects and has attracted much attention in the construction of sensors because of its special spiral structure and the easy preparation of the one-dimensional PC structure [26]. It is a liquid crystal with photonic bandgap properties and a strong spin, pronounced circular dichroism and selective reflection of light that can be seen very clearly with the naked eye as a change in color [27,28]. The molecules are arranged in parallel layers in the plane and the orientation of the molecules in the adjacent layers varies helically in the direction normal to the plane. The color reflected by the CLC photonic crystal is related to its pitch [29]. The pitch of the cholesteric phase liquid crystal can be regulated by simply changing the concentration of chiral molecules doped during the preparation process, and can be polymerized into stable films under UV illumination. The prepared solid film is easy to preserve and transport, making it very widely used [30,31].

The CLC PC films are mainly used to detect volatile organic compounds (VOC) based on the change in pitch size in the microstructure, resulting in the obvious color variation of the films on the macroscopic level [32,33]. Recently, a widely used stimulus-responsive CLC PC film was constructed by combining the responsive functional materials with CLC PC. The optical signal of the CLC PC sensor can be changed by different physical factors such as pressure, temperature and humidity [34–36]. In addition, biological or chemical reactions can be initiated in the CLC PC films to achieve the analysis and detection of specific targets [37–40].

Polyacrylic acid (PAA) hydrogel is a polymer material with an interpenetrating three-dimensional network structure. The molecular chain of PAA contains a large number of ionizable COOH groups and is therefore a pH-sensitive smart polymer. When the pH value of the solution is higher than the pKa of acrylic acid, COOH is dissociated, the free energy of the system is reduced, and the gel swells by absorption; when the pH is lower than the pKa of acrylic acid, due to the hydrogen bonding between COOH, in this case the conformation of the PAA molecular chain is curled compared with the high pH. Under this condition, the hydrophilicity of the PAA is relatively weaker and its hydrophobicity is relatively stronger. Therefore, the swelling degree of the gel is reduced [41,42] and it possesses obvious reversible shrinkage or expansion ability under pH variation [43].

In recent years, several groups have designed and prepared a series of responsive photonic gels based on the property that responsive gels produce strong volume expansion and contraction when stimulated by external conditions [44–46]. As such, photonic crystal hydrogels, the most prevalent of the gels, have become one of the research hotspots in the field of sensing technology. By introducing polymer hydrogels into arrays of crystallized colloidal microspheres (e.g., silica, polystyrene microspheres), hydrogel complexes with a controlled and ordered photonic band gap structure can be formed. Changes in the external environment can lead to expansion or contraction in the volume of the polymer hydrogel, which in turn leads to changes in the lattice spacing of the colloidal microsphere array, displacing the Bragg diffraction peak and leading to color changes in the photonic crystal hydrogel [47–49]. Photonic crystal gels have been used to detect mercury ions and other substances and have shown good response properties [50,51]. CLC with better optical properties is relatively simple to prepare, and more sensitive to color changes compared with other photonic crystals. Stumpel et al. [31] prepared a stimulus-responsive cholesteric liquid crystal-hydrogel polymer network (CLC-PAA) material by using the PAA hydrogel and the CLC PC structure. The color of CLC-PAA hydrogel film was changed, obviously caused by the increase or decrease in the CLC pitch through the swell or contract of the PAA hydrogel when the pH was changed.

Herein, a method for detecting Hg^{2+} is proposed by using a cholesteric liquid crystal photonic hydrogel film immobilized with urease (CLC-PAA_{urease} film as a sensitive recognition element. As shown in Figure 1, urease can catalyze the hydrolysis of urea and produce NH_3 , leading to an elevated pH in the PAA hydrogel. The PAA hydrogel belongs

to a class of pH-sensitive anionic hydrogels with abundant -COOH on its chain skeleton. The hydrogel has a higher swelling rate at a higher pH, causing an increase in the pitch of the photonic crystal, resulting in the red shift of its diffraction wavelength. In contrast, in the absence of Hg^{2+} , the hydrolysis of urea by urease is blocked because the urease activity is inhibited. At the same time, the color of the CLC-PAA PC film changes slowly, and detection of the target Hg^{2+} can be realized based on the shift of the reflected light wavelength of the film.

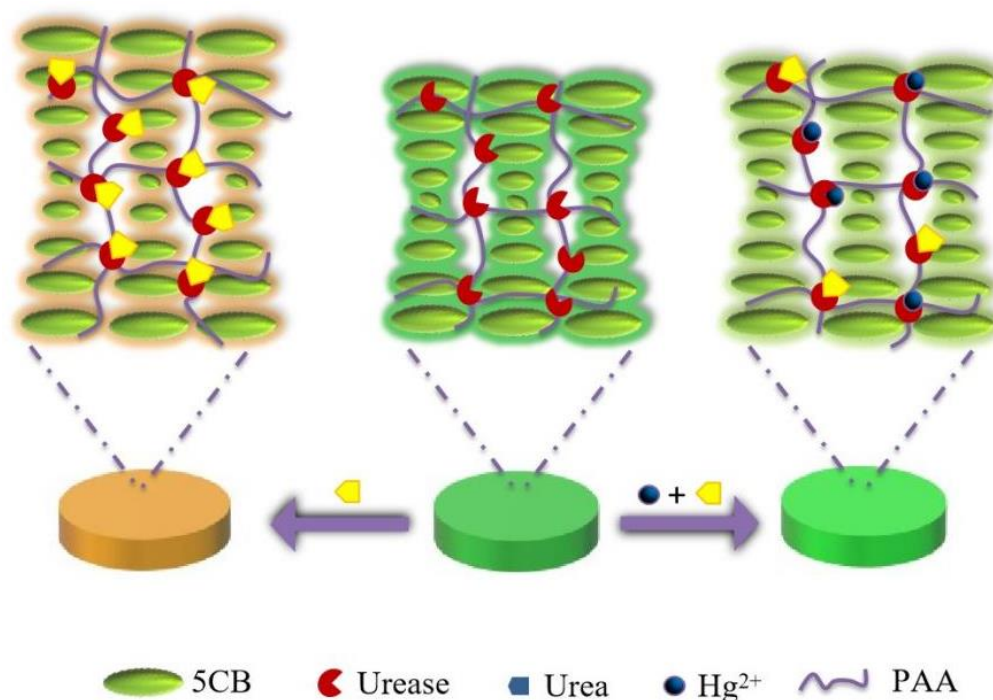


Figure 1. Schematic diagram of CLC-PAA urease PC films for the detection of Hg^{2+} .

2. Materials and Methods

2.1. Experimental Materials

2-(N-Morpholino) ethanesulfonic acid (MES) was purchased from Shanghai Acme Chemical Co., Ltd. (Shanghai, China). N-Hydroxysuccinimide (NHS), urea and urease (Jack Bean) were provided by Shanghai Yuanye Bio-Technology Co., Ltd. (Shanghai, China). 1-(3-Dimethylaminopropyl)-3-ethylcarbodiimide hydrochloride was purchased from Macklin Biochemical Co., Ltd. (Shanghai, China). 1,4-Bis-[4-(3-Acryloyloxypropoxy) benzoyloxy]-2-methylbenzene (RM257) was provided by Bide Pharmatech Ltd. (Shanghai, China) (S)-4'-(2-Methylbutyl)-[1,1'-biphenyl]-4-carbonitrile (CB15) and acrylic acid (AA) were ordered from Sigma-Aldrich company (St. Louis, MO, USA). α -Hydroxyisobutyryl benzene (Irgacure 1173) was provided by Shanghai Darui Fine Chemical Co., Ltd. (Shanghai, China). Tripropanediol diacrylate (TPGDA) was purchased from Heowns Biochem Technologies LLC., Tianjin, China. Mercury ion standard solution (100 $\mu\text{g}/\text{mL}$) was purchased from Shanghai Acme Chemical Co., Ltd. (Shanghai, China). Trometamol (Tris) was purchased from Sangon Biotech Co., Ltd. (Shanghai, China). N, N-Dimethyl-N-octadecyl (3-aminopropyl)trimethoxysilyl chloride (DMOAP) was provided by Energy Chemical Co., Ltd. (Shandong, China). Potassium hydroxide (KOH) and acetone were purchased from Laiyang Kangde Chemicals Co., Ltd. (Shandong, China). Nitrogen was ordered from Jinan Deyang Special Gas Co., Ltd. (Shandong, China). Methanol and ethanol were purchased from Tianjin Fuyu Fine Chemical Co., Ltd. (Tianjin, China). All the chemicals were used without further purification.

2.2. Experimental Apparatus

Cary 5000 UV–Vis spectrophotometer (Agilent, Palo Alto, CA, USA) was used to characterize the reflectance spectra of CLC-PAA photonic crystal gel films with a resolution better than 0.048 nm. Tensor II FTIR (Bruker, Germany) was employed to characterize the successful cross-linking of urease in CLC-PAA photonic crystal gel films using potassium bromide pressed slices with a resolution better than 0.4 cm^{-1} . JSEM-6700F scanning electron microscope (JEOL, Tokyo, Japan) was used to observe the changes in the cut surface morphology of CLC films before and after cross-linking with PAA. The prepared films were fixed to the silicon wafer using conductive adhesive and the surface of the composite film was sprayed with gold to enhance its electrical conductivity before testing. AG-2000A Tensile tester (SHMADZU, Tokyo, Japan) was utilized to test the tensile properties of CLC, PAA and CLC-PAA films.

2.3. Preparation of Hydrogel

The precursor of PAA hydrogel was composed of AA, TPGDA and Irgacure 1173, which should be kept in a dark place. The glass slides were cleaned with cleaning agent to remove the oil stain on the surface, then cleaned with a large amount of ultra pure water, methanol, and ethanol, respectively. Finally, the glass slides were dried with nitrogen in the oven at $110\text{ }^{\circ}\text{C}$ for 1 h and were then kept in a desiccator. The cleaned glass slides were cut into square glasses which were used for the preparation of PAA hydrogel films.

2.4. Preparation of CLC Photonic Crystal Film

We obtained the color liquid crystals (CLC photonic crystal) by mixing chiral dopant (CB15) and RM257 in a certain proportion at $60\text{ }^{\circ}\text{C}$ for 6 h. Then, a small amount of CLC photonic crystal was placed in the center of the glass slide, another slide was covered, and the two ends of the two slides were fixed by a long-tail clamp. Finally, we obtained the CLC photonic crystal films by UV polymerization through a portable ultraviolet (UV) lamp (365 nm) for 10 min.

2.5. Preparation of CLC-PAA Photonic Crystal Gel Film

The prepared CLC photonic crystal films were continuously cleaned and soaked in acetone to completely remove the chiral dopant (CB15). Then, the precursor of PAA hydrogel was immersed in the CLC photonic crystal films which removed the chiral dopant. The thickness of the film was controlled by the long tail clamp. Finally, we obtained the CLC-PAA photonic crystal film using the portable UV lamp for 10 min.

2.6. Preparation of CLC-PAA_{urease} PC Film

The excess AA on the CLC-PAA photonic crystal film was removed using a large amount of water in order to activate the carboxyl group on the prepared films that were placed in EDC/NHS (0.2 M/0.2 M) MES buffer solution. Next, they were incubated with the urease in PBS buffer for 1 h at room temperature. Finally, we used a large amount of PBS buffer for flushing out the films, and they were dried naturally at room temperature to obtain the CLC-PAA photonic crystal gel film with immobilized urease (CLC-PAA_{urease} PC film).

2.7. Detection of Hg²⁺

The CLC-PAA_{urease} PC film was used to detect Hg²⁺. The different concentrations of Hg²⁺ solutions were dropped on the prepared films to inhibit the activity of urease. Then, we placed the rinsed off Hg²⁺ films in a urea solution (10 mM) for 10 min at room temperature. Then, the films that inhibited urease activity were reacted with urea for 10 min. Finally, we obtained the concentrations of Hg²⁺ through the wavelengths of the reflected light of these films by UV–vis spectra. To verify the selectivity of the CLC-PAA_{urease} PC film, Hg²⁺ was replaced by Ca²⁺, Cu²⁺, Zn²⁺, Al³⁺ and Fe³⁺ with other conditions unchanged.

3. Results and Discussion

3.1. Subsection Structure Characterization of CLC-PAA PC Films

It is reported that PAA hydrogels possess a rapid pH response, good biocompatibility, and an interpenetrating network structure. The PAA hydrogels were cross-linked in the CLC PC films to enable the pH responsiveness of the materials. Firstly, we prepared the PAA hydrogel film and explored its properties. Figure 2 shows that the prepared PAA hydrogel film has an obvious swelling property in water. As we see in Figure 3a, the swelling ratio (φ) of the PAA film is a function of the amount of TPGDA (ζ). It was found that φ reaches a maximum when the value of ζ is 0.5 wt%. However, φ decreases at the ζ of more than 0.5 wt% due to the cross-linked structure. Therefore, the optimum condition of TPGDA for the preparation of the PAA hydrogel film was 0.5% which was selected to carry out the subsequent experiments. Figure 2b shows φ of the PAA hydrogel film ($\zeta = 0.5$ wt%) at different pH. Apparently, within the pH range investigated, the values of φ increase as the pH increases (Figure 3b).

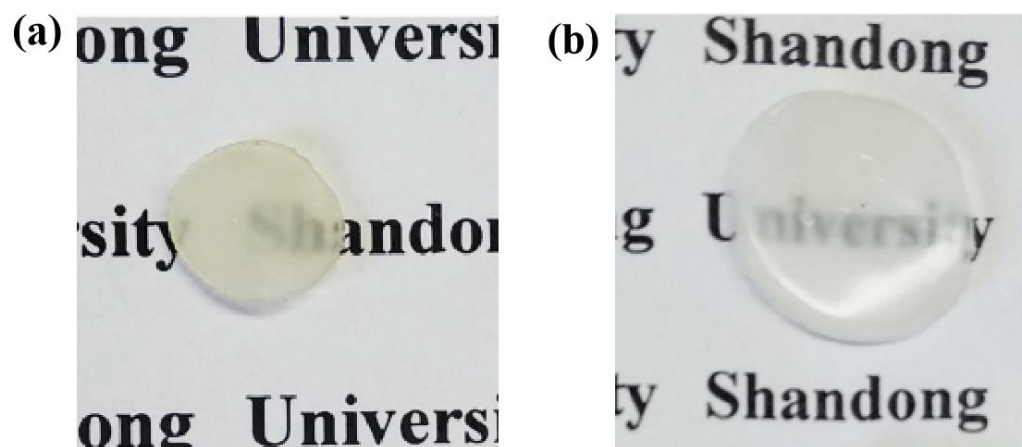


Figure 2. Comparison diagram of PAA gel film in water: (a) before and (b) after the swelling.

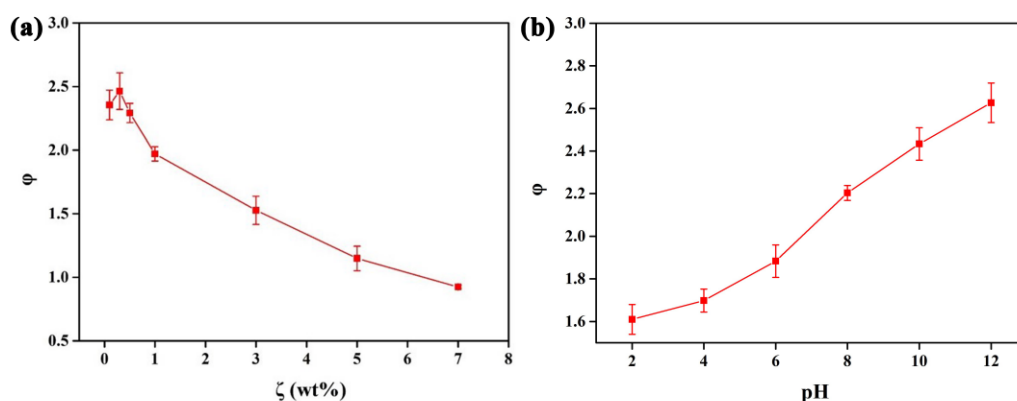


Figure 3. Swelling ratio (φ) of PAA gel film (a) at different amounts of TPGDA (ζ) and (b) at different pH. φ is defined as $(m_2 - m_1)/m_1$, where m_2 and m_1 are the mass of gel film in water and dry state, respectively.

Subsequently, we prepared the CLC photonic crystal films with a flat surface (Figure 4a) and a thickness of about 26.69 μm (Figure 4b). Then, we processed the above films (the chiral dopant CB15 was removed and PAA was crosslinked) to prepare the CLC-PAA photonic crystal gel film. As can be seen from the UV-visible spectrum in Figure 4c, there is a significant red shift in the wavelength of the reflected light from the films after the removal of the chiral dopant CB15 and cross-linking of the PAA. In addition, the inset of Figure 4c shows photographic images of the extracted CLC PC CB15 solid film, the CLC PC

film and the CLC-PAA PC film. They show blue, blue-green, and green colors, respectively, indicating that the AA/TPGDA was successfully penetrated and UV-cured in the CLC PC films.

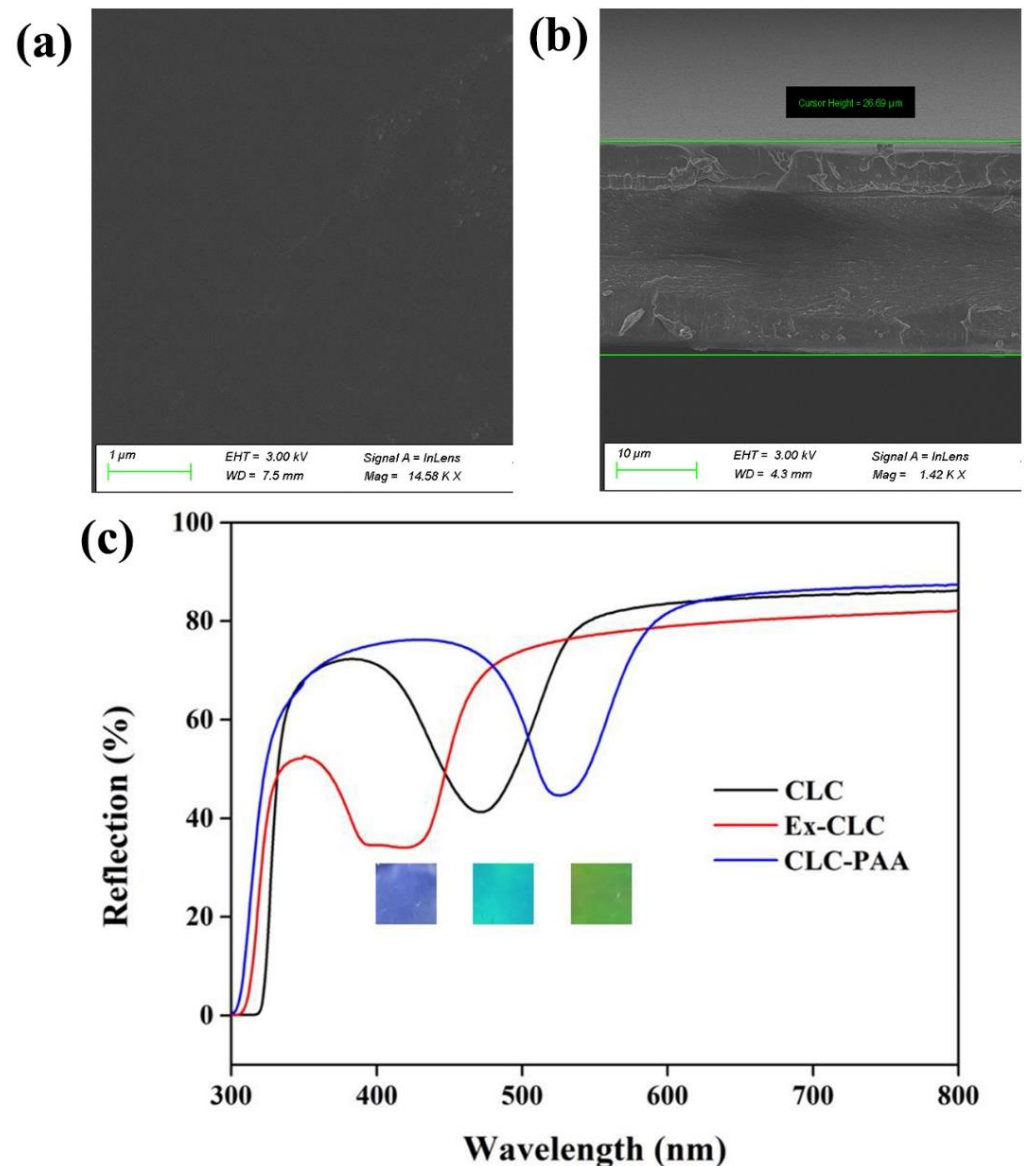


Figure 4. SEM images of (a) fractured surface and (b) the upper surface of prepared CLC PC films. (c) UV-vis spectra and the optical photographs of Ex-CLC, CLC PC and CLC-PAA PC film.

Figure 5a,b separately show the SEM images of the cross-section surface of the CLC PC film before and after the infiltration and crosslinking of the AA/TPGDA (CLC-PAA PC hydrogel film), which displays a significant change in the pitch of the helix. In addition, with the participation of the PAA, the pitch of the PC film becomes larger and its serrated structure grows thicker after cross-linking the hydrogel, which are the characteristics of the structural properties of the PAA hydrogel. Therefore, the PAA hydrogels were successfully cross-linked into the CLC PC films.

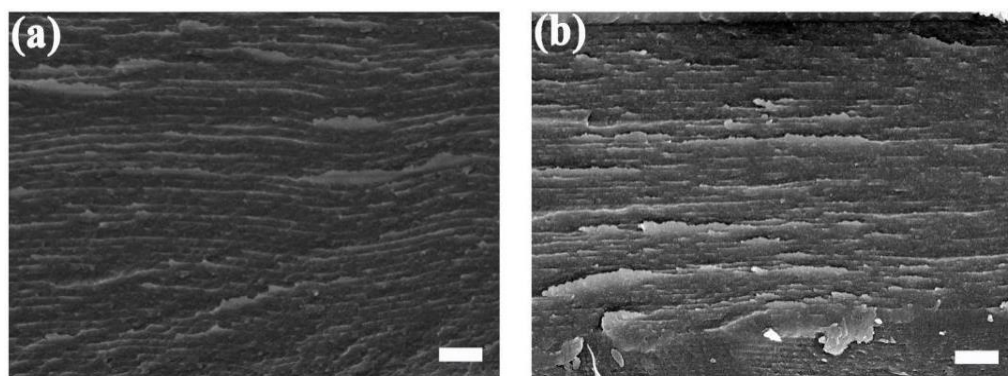


Figure 5. SEM images of fractured surface of (a) CLC film and (b) CLC-PAA photonic crystal hydrogel film when the films were cut perpendicularly to the surface of films. scale bar: 1 μm .

Subsequently, we measured the tension–strain curves of the CLC, PAA and CLC-PAA films, which indicated that the mechanical properties of the CLC films were improved after the AA/TPGDA was cross-linked by the CLC films (Figure 6). It follows that the PAA hydrogel was introduced into the CLC film successfully. This remarkably improved the mechanical strength of the CLC film, which facilitates the reusability of the film in analytical assays.

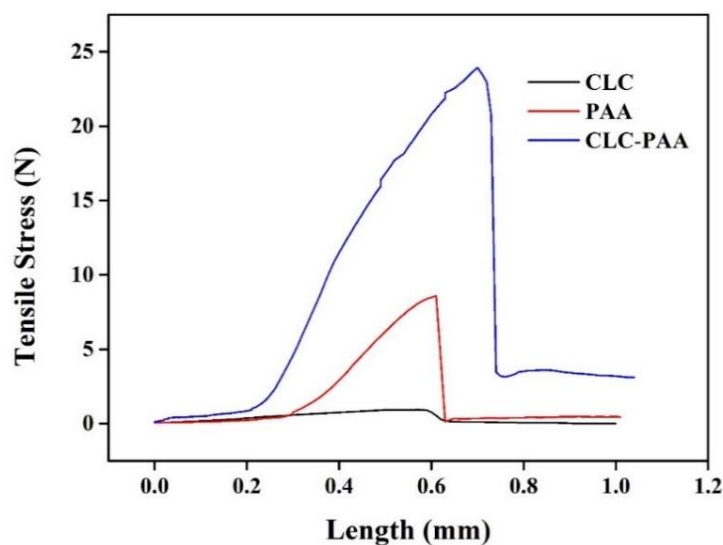


Figure 6. Tensile stress–strain curves of CLC, PAA and CLC-PAA films.

3.2. PH Response of CLC-PAA PC Films

The pH response of the CLC-PAA PC films is shown in Figure 7. As expected, the color of the prepared films changed distinctly from green to orange-yellow when the experimental conditions were changed from pH = 4 to pH = 12. Furthermore, the wavelength of the reflected light increases as the pH increases, which shows an obvious redshift. This result indicates that the PAA hydrogels expand at a high pH and correspondingly increase the helix pitch of the CLC PC films. Thus, local pH changes can be employed in the CLC-PAA films for sensor construction, which can be used to detect heavy metal ions without sophisticated instruments.

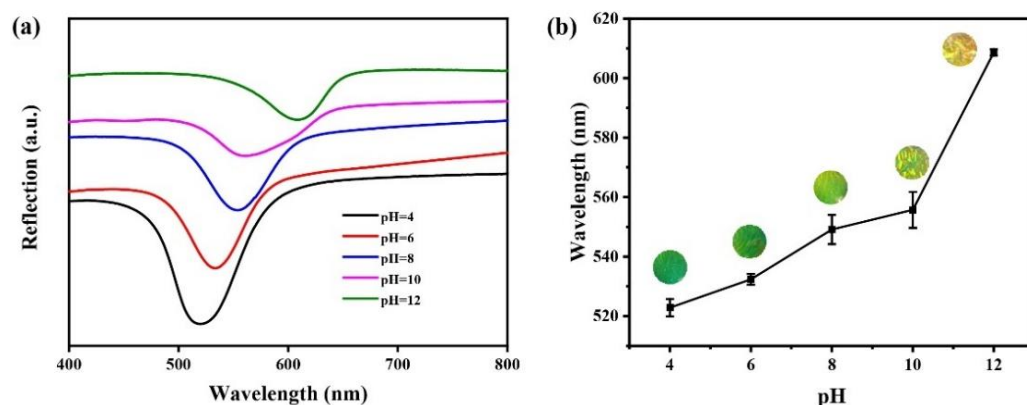


Figure 7. (a) UV-visible reflection spectra of CLC-PAA PC films at different pH; (b) The wavelengths of the reflection light and the optical images of CLC-PAA PC films under different pH.

3.3. Crosslinking of Urease on the CLC-PAA PC Films

We studied the structure of the CLC-PAA PC films and the urease immobilization using Fourier transform infrared (FTIR) spectroscopy. The FTIR spectrum of the CLC solid films (Figure 8a) shows $-\text{CH}_2-$, $-\text{C}=\text{O}$, $-\text{Ar}-\text{O}-$, and $-\text{Ar}-$ stretching bands at 2839 , 1720 , 1257 , and 840 cm^{-1} , respectively. These peaks may result from RM257. The FTIR spectrum of the CLC-PAA hydrogel films (Figure 8b) shows the same peaks as the CLC solid film with new peaks derived from the PAA hydrogel. For example, new peaks appear at $1700\text{--}1800\text{ cm}^{-1}$ and $1415\text{--}1440\text{ cm}^{-1}$, which are attributed to the $-\text{C}=\text{O}$ and the carboxylic acid groups, indicating the PAA hydrogel is cross-linked in the CLC PC films. Figure 8c shows the FTIR spectrum of the CLC-PAA hydrogel films immobilized with urease (CLC-PAA_{urease} films). The new peak at $3000\text{--}3700\text{ cm}^{-1}$ represents the amide bands from the urease. Thus, it is obvious that urease was successfully immobilized in the CLC-PAA hydrogel films.

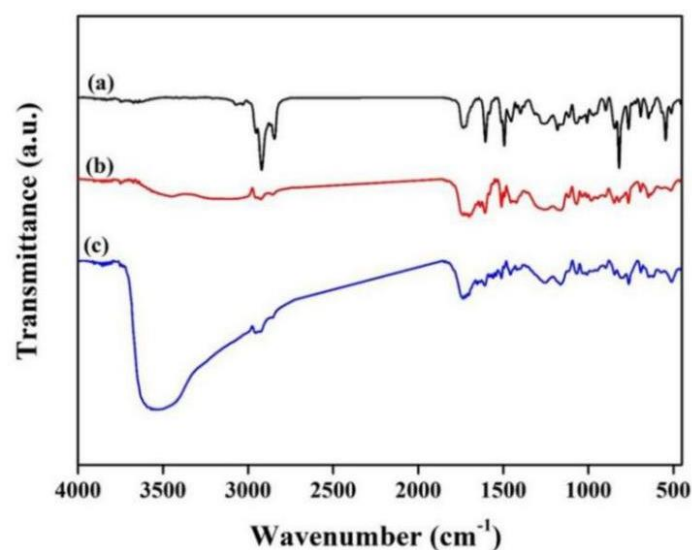


Figure 8. FTIR spectra of (a) CLC PC films, (b) CLC-PAA PC films, and (c) CLC-PAA_{urease} PC films, respectively.

3.4. Optimization of Experimental Conditions

The concentration of urea plays a significant role in the sensitivity of Hg^{2+} detection. Thus, we investigated the variation of the wavelength value of the maximum reflection peak of the CLC-PAA_{urease} PC films by the immobilized urease (1000 U/mL) with different urea concentrations (Figure 9). It was found that the wavelength value of the maximum reflection peak of the CLC-PAA_{urease} PC films appeared red-shifted, whereas the wave-

length value stayed stable at 10 mM, 50 mM, and 100 mM, respectively. Therefore, we fixed the concentration of urea at 10 mM in the subsequent experiments. In addition, we also studied the responses of the CLC-PAA_{urease} PC films in the same observation time (10 min) to the solutions of urea (10 mM) at the different concentrations of urease. Figure 10a shows the UV-Vis spectra of the CLC-PAA_{urease} PC films at different urease concentrations. It can be clearly observed that the wavelength location corresponding to the maximum reflection peak was red shifted (Figure 10b) and the color of the films changed from green to orange with the increasing urease concentration (Figure 10c). It was also revealed that within the investigated concentration range, the response signal of the films reached the platform period when the concentration of urease was greater than or equal to 800 U/mL. Therefore, we chose the concentration of urease at 800 U/mL as the optimal condition.

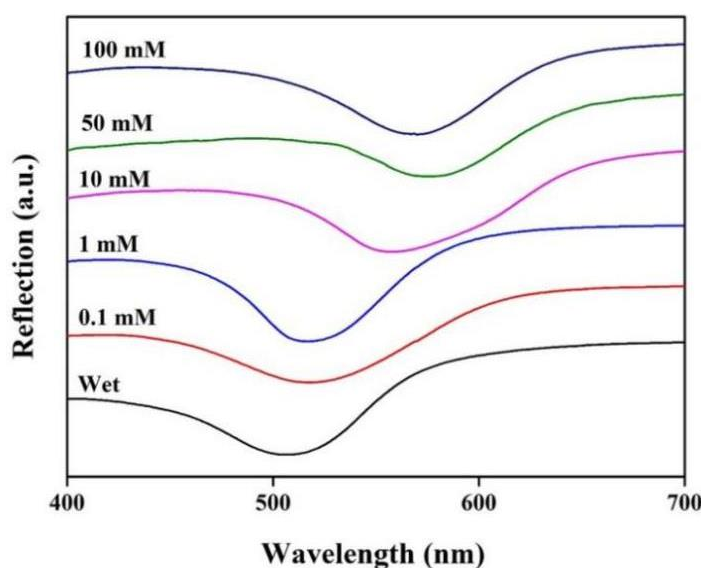


Figure 9. UV-visible reflection spectra of CLC-PAA_{urease} photonic crystal hydrogel films after dropping urea solution (200 μ L) with different concentrations for 10 min.

3.5. Sensitivity and Specificity of CLC-PAA Urease PC Films for Hg²⁺ Detection

We explored the responses of the wavelength value of the maximum reflection peak coupled to different concentrations of Hg²⁺ with the prepared CLC-PAA_{urease} PC films (Figure 11a). It is clear that Hg²⁺ can inhibit the activity of urease, resulting in a change in the microenvironment of the prepared films. It was found that the wavelength value of the reflection spectrum showed an obvious blue shift when increasing the concentration of Hg²⁺. The wavelength value of the reflected light of the prepared films did not change at 10 nM, which was considered to be the detection limit of Hg²⁺ (Figure 11b). The color of the film gradually changes from yellow-green to blue (Figure 11c). Finally, we explored the specificity of the prepared films for the detection of Hg²⁺. As seen in Figure 12, when Hg²⁺ is present, the changes in the UV-visible reflection spectra wavelength of the CLC-PAA_{urease} PC films are obviously observed compared with the blank and other metal ions. This result clearly reveals the specificity of the proposed method in the detection of Hg²⁺.

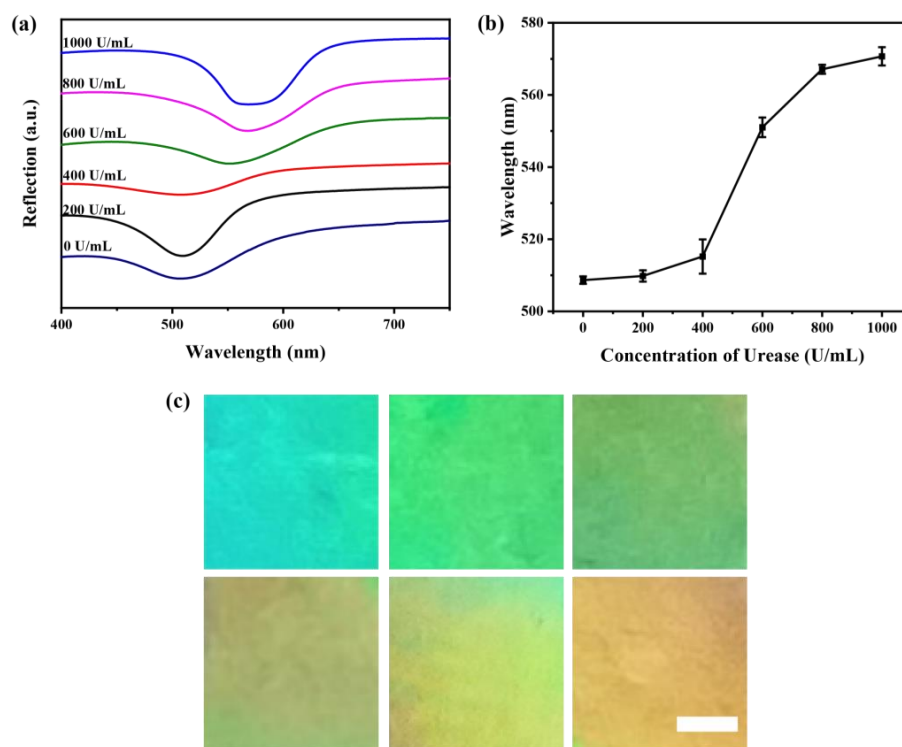


Figure 10. (a) The UV-visible reflection spectra of CLC-PAA PC films at different concentrations of urease (The films were treated with 10 mM urea for 10 min.); (b) The wavelength values of the reflection light; (c) The optical images of CLC-PAA PC films at different concentrations of urease. scale bar: 1 mm.

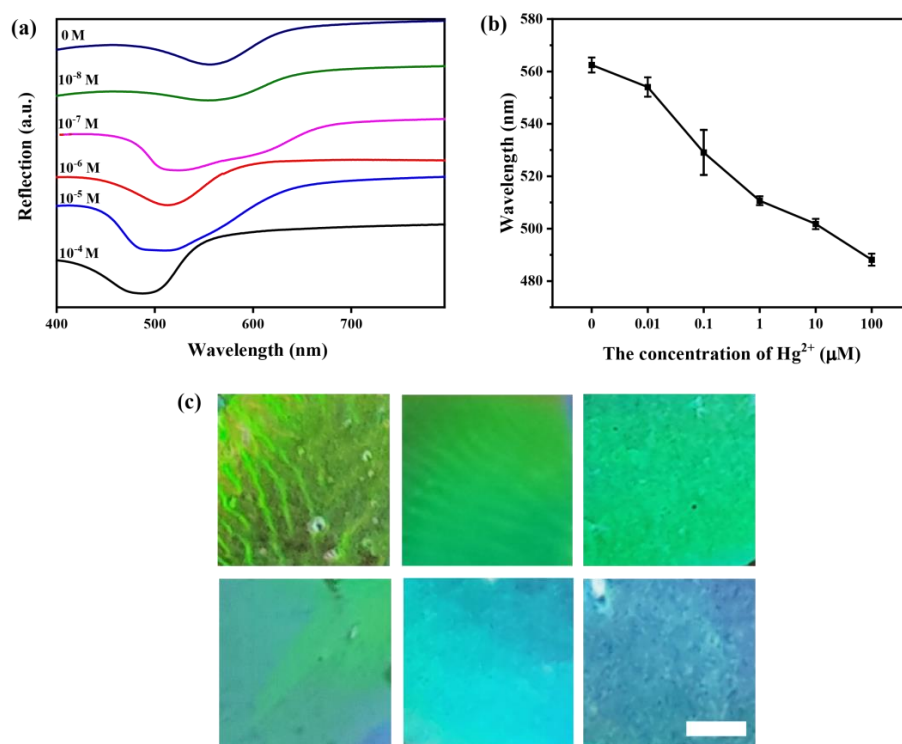


Figure 11. (a) The UV-visible reflection spectra of CLC-PAA_{urease} PC films at different concentrations of Hg^{2+} (The films were treated with 10 mM urea for 10 min.); (b) The wavelength values of the reflection light of CLC-PAA_{urease} PC films at different concentrations of Hg^{2+} ; (c) The optical images of CLC-PAA_{urease} PC films at different concentrations of Hg^{2+} . scale bar: 1 mm.

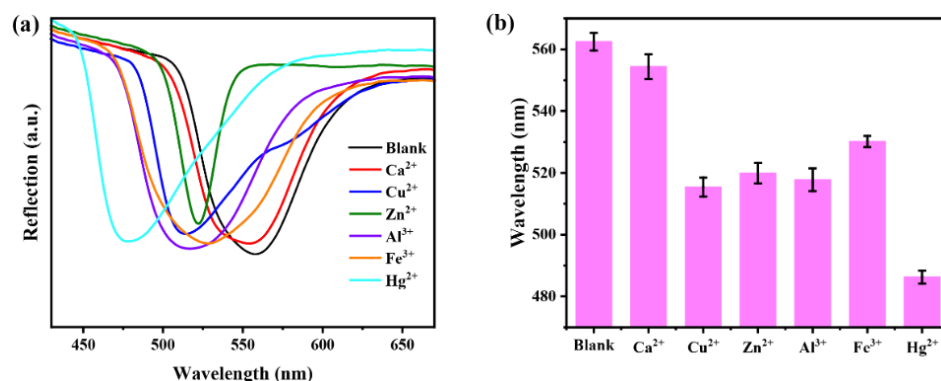


Figure 12. (a) UV-visible reflection spectra of CLC-PAA_{urease} PC films with various metal ions (The films were treated with urea (10 mM) for 10 min); (b) The wavelength values of the reflected light of CLC-PAA_{urease} PC films with various metal ions.

4. Conclusions

In summary, a simple, portable and new strategy has been developed for the detection of Hg²⁺ based on CLC-PAA_{urease} PC films. The detection limit of Hg²⁺ is as low as 10 nM. This method immobilized urease on CLC-PAA PC films and changed the optical signal of the prepared films by the enzymatic hydrolysis of urea leading to variation in the microenvironment. The reflected wavelength is directly used as the detection signal of the films. The proposed strategy is very promising in the evaluation of environmental water.

Author Contributions: Conceptualization, resources, supervision, project administration, funding acquisition, L.Y.; methodology, writing—original draft preparation, J.L.; investigation, visualization, W.T.; data curation, formal analysis, J.S.; validation, visualization, D.W. All authors have read and agreed to the published version of the manuscript.

Funding: This research was funded by the National Natural Science Foundation of China (No. 21972074).

Institutional Review Board Statement: Not applicable.

Informed Consent Statement: Not applicable.

Data Availability Statement: Not applicable.

Acknowledgments: Li Yu acknowledges financial support from the National Natural Science Foundation of China.

Conflicts of Interest: The authors declare no conflict of interest.

References

- Zhou, Z.; Yan, R.; Zhao, J.; Zhao, J.; Yang, L.; Chen, J.; Hu, Y.; Jiang, F.; Liu, Y. Highly selective and sensitive detection of Hg²⁺ based on fluorescence enhancement of Mn-doped ZnSe QDs by Hg²⁺-Mn²⁺ replacement. *Sens. Actuators B Chem.* **2018**, *254*, 8–15. [[CrossRef](#)]
- Gao, P.; Lei, J.; Tan, J.; Wang, G.; Liu, H.; Zhou, L. Self-assembled magnetic microcrystalline cellulose/MoS₂/Fe₃O₄ composite for efficient adsorptive removal of mercury ions (Hg²⁺). *Compos. Commun.* **2021**, *25*, 100736. [[CrossRef](#)]
- Mermer, Z.; Yavuz, O.; Atasen, S.K.; Alcay, Y.; Yilmaz, I. Architecture of multi-channel and easy-to-make sensors for selective and sensitive Hg²⁺ ion recognition through HgC and HgN bonds of naphthoquinone-aniline/pyrene union. *J. Hazard. Mater.* **2021**, *410*, 124597. [[CrossRef](#)] [[PubMed](#)]
- Tian, C.; Zhao, L.; Zhu, J.; Zhang, S. Ultrasensitive detection of trace Hg²⁺ by SERS aptasensor based on dual recycling amplification in water environment. *J. Hazard. Mater.* **2021**, *416*, 126251. [[CrossRef](#)]
- Song, W.; Xiong, H.; Qi, R.; Wang, S.; Yang, Y. Effect of salinity and algae biomass on mercury cycling genes and bacterial communities in sediments under mercury contamination: Implications of the mercury cycle in arid regions. *Environ. Pollut.* **2021**, *269*, 116141. [[CrossRef](#)]
- Ma, M.; Du, H.; Wang, D. Mercury methylation by anaerobic microorganisms: A review. *Crit. Rev. Environ. Sci. Technol.* **2019**, *49*, 1893–1936. [[CrossRef](#)]

7. Song, C.; Yang, B.; Zhu, Y.; Yang, Y.; Wang, L. Ultrasensitive silver nanorods array SERS sensor for mercury ions. *Biosens. Bioelectron.* **2017**, *87*, 59–65. [[CrossRef](#)]
8. Oh, S.; Jeon, J.; Jeong, J.; Park, J.; Oh, E.-T.; Park, H.J.; Lee, K.-H. Fluorescent Detection of Methyl Mercury in Aqueous Solution and Live Cells Using Fluorescent Probe and Micelle Systems. *Anal. Chem.* **2020**, *92*, 4917–4925. [[CrossRef](#)]
9. Guzzi, G.; Ronchi, A.; Pigatto, P. Toxic effects of mercury in humans and mammals. *Chemosphere* **2021**, *263*, 127990. [[CrossRef](#)]
10. Lei, Y.; Zhang, F.; Guan, P.; Guo, P.; Wang, G. Rapid and selective detection of Hg(II) in water using AuNP in situ-modified filter paper by a head-space solid phase extraction Zeeman atomic absorption spectroscopy method. *New J. Chem.* **2020**, *44*, 14299–14305. [[CrossRef](#)]
11. Hsu, I.H.; Hsu, T.-C.; Sun, Y.-C. Gold-nanoparticle-based graphite furnace atomic absorption spectrometry amplification and magnetic separation method for sensitive detection of mercuric ions. *Biosens. Bioelectron.* **2011**, *26*, 4605–4609. [[CrossRef](#)] [[PubMed](#)]
12. Wang, Z.; Wu, D.; Wu, G.; Yang, N.; Wu, A. Modifying Fe₃O₄ microspheres with rhodamine hydrazide for selective detection and removal of Hg²⁺ ion in water. *J. Hazard. Mater.* **2013**, *244*, 621–627. [[CrossRef](#)] [[PubMed](#)]
13. Paglia, G.; Miedico, O.; Tarallo, M.; Lovino, A.R.; Astarita, G.; Chiaravalle, A.E.; Corso, C. Evaluation of seasonal variability of toxic and essential elements in urine analyzed by inductively coupled plasma mass spectrometry. *Expos. Health* **2016**, *9*, 79–88. [[CrossRef](#)]
14. Shih, T.-T.; Chen, J.-Y.; Luo, Y.-T.; Lin, C.-H.; Liu, Y.-H.; Su, Y.-A.; Chao, P.-C.; Sun, Y.-C. Development of a titanium dioxide-assisted preconcentration/on-site vapor-generation chip hyphenated with inductively coupled plasma-mass spectrometry for online determination of mercuric ions in urine samples. *Anal. Chim. Acta* **2019**, *1063*, 82–90. [[CrossRef](#)] [[PubMed](#)]
15. Surucu, O. Electrochemical removal and simultaneous sensing of mercury with inductively coupled plasma-mass spectrometry from drinking water. *Mater. Today Chem.* **2022**, *23*, 100639. [[CrossRef](#)]
16. Fu, L.; Zhuang, J.; Tang, D.; Que, X.; Lai, W.; Chen, G. DNA pseudoknot-functionalized sensing platform for chemoselective analysis of mercury ions. *Analyst* **2012**, *137*, 4425–4427. [[CrossRef](#)]
17. He, W.; Qiao, B.; Li, F.; Pan, L.; Chen, D.; Cao, Y.; Tu, J.; Wang, X.; Lv, C.; Wu, Q. A novel electrochemical biosensor for ultrasensitive Hg²⁺ detection via a triple signal amplification strategy. *Chem. Commun.* **2021**, *57*, 619–622. [[CrossRef](#)]
18. Wang, L.; Yang, Y.; Liang, H.; Pan, L.; Chen, D.; Cao, Y.; Tu, J.; Wang, X.; Lv, C.; Wu, Q. A novel N,S-rich COF and its derived hollow N,S-doped carbon@Pd nanorods for electrochemical detection of Hg²⁺ and paracetamol. *J. Hazard. Mater.* **2021**, *409*, 124528. [[CrossRef](#)]
19. Qi, J.; Li, B.; Wang, X.; Zhang, Z.; Wang, Z.; Han, J.; Chen, L. Three-dimensional paper-based microfluidic chip device for multiplexed fluorescence detection of Cu²⁺ and Hg²⁺ ions based on ion imprinting technology. *Sens. Actuators B Chem.* **2017**, *251*, 224–233. [[CrossRef](#)]
20. Peng, D.; Zhang, L.; Liang, R.-P.; Qiu, J.-D. Rapid Detection of Mercury Ions Based on Nitrogen-Doped Graphene Quantum Dots Accelerating Formation of Manganese Porphyrin. *ACS Sens.* **2018**, *3*, 1040–1047. [[CrossRef](#)]
21. Wang, J.; Du, C.; Yu, P.; Zhang, Q.; Li, H.; Sun, C. A label-free and enzyme-free fluorescent assay for mercury ions based on T-Hg(II)-T nanoladders and DNA-templated silver nanoclusters/graphene oxide nanocomposites. *Sens. Actuators B Chem.* **2021**, *348*, 130707. [[CrossRef](#)]
22. Lim, J.W.; Kim, T.Y.; Choi, S.W.; Woo, M.A. 3D-printed rolling circle amplification chip for on-site colorimetric detection of inorganic mercury in drinking water. *Food Chem.* **2019**, *300*, 125177. [[CrossRef](#)] [[PubMed](#)]
23. Tokunaga, S.; Itoh, Y.; Tanaka, H.; Araoka, F.; Aida, T. Redox-responsive chiral dopant for quick electrochemical color modulation of cholesteric liquid crystal. *J. Am. Chem. Soc.* **2018**, *140*, 10946–10949. [[CrossRef](#)] [[PubMed](#)]
24. Kelly, J.A.; Shukaliak, A.M.; Cheung, C.C.; Shopsowitz, K.E.; Hamad, W.Y.; MacLachlan, M.J. Responsive photonic hydrogels based on nanocrystalline cellulose. *Angew. Chem. Int. Ed.* **2013**, *52*, 8912–8916. [[CrossRef](#)]
25. Haque, M.A.; Kamita, G.; Kurokawa, T.; Tsujii, K.; Gong, J. Unidirectional alignment of lamellar bilayer in hydrogel: One-dimensional swelling, anisotropic modulus, and stress/strain tunable structural color. *Adv. Mater.* **2010**, *22*, 5110–5114. [[CrossRef](#)]
26. Seo, H.J.; Lee, S.S.; Noh, J.; Ka, J.-W.; Won, J.C.; Park, C.; Kim, S.-H.; Kim, Y.H. Robust photonic microparticles comprising cholesteric liquid crystals for anti-forgery materials. *J. Mater. Chem. C* **2017**, *5*, 7567–7573. [[CrossRef](#)]
27. Dierking, I. Chiral Liquid Crystals: Structures, Phases, Effects. *Symmetry* **2014**, *6*, 444–472. [[CrossRef](#)]
28. Ding, H.; Zhu, C.; Tian, L.; Liu, C.; Fu, G.; Shang, L.; Gu, Z. Structural Color Patterns by Electrohydrodynamic Jet Printed Photonic Crystals. *ACS Appl. Mater. Interfaces* **2017**, *9*, 11933–11941.
29. Lim, J.S.; Kim, Y.J.; Park, S.Y. Functional solid-state photonic droplets with interpenetrating polymer network and their applications to biosensors. *Sens. Actuators B Chem.* **2021**, *329*, 129165. [[CrossRef](#)]
30. Chen, G.; Wang, L.; Wang, Q.; Sun, J.; Song, P.; Chen, X.; Liu, X.; Guan, S.; Zhang, X.; Wang, L.; et al. Photoinduced Hyper-Reflective Laminated Liquid Crystal Film with Simultaneous Multicolor Reflection. *ACS Appl. Mater. Interfaces* **2014**, *6*, 1380–1384. [[CrossRef](#)]
31. Stumpel, J.E.; Gil, E.R.; Spoelstra, A.B.; Bastiaansen, C.M.; Broer, D.J.; Schenning, A.J. Stimuli-responsive materials based on interpenetrating polymer liquid crystal hydrogels. *Adv. Funct. Mater.* **2015**, *25*, 3314–3320. [[CrossRef](#)]
32. Chang, C.K.; Kuo, H.L.; Tang, K.T.; Chiu, S.W. Optical detection of organic vapors using cholesteric liquid crystals. *Appl. Phys. Lett.* **2011**, *99*, 073504. [[CrossRef](#)]

33. Mujahid, A.; Stathopoulos, H.; Lieberzeit, P.A.; Dickert, F.L. Solvent vapour detection with cholesteric liquid crystals-optical and mass-sensitive evaluation of the sensor mechanism. *Sensors* **2010**, *10*, 4887–4897. [[CrossRef](#)] [[PubMed](#)]
34. Cho, S.; Li, Y.; Seo, M.; Kumacheva, E. Nanofibrillar Stimulus-Responsive Cholesteric Microgels with Catalytic Properties. *Angew. Chem. Int. Ed.* **2016**, *55*, 14014–14018. [[CrossRef](#)]
35. Zhang, P.; Kragt, A.J.; Schenning, A.J.; Haan, L.D.; Zhou, G. An easily coatable temperature responsive cholesteric liquid crystal oligomer for making structural color patterns. *J. Mater. Chem. C* **2018**, *6*, 7184–7187. [[CrossRef](#)]
36. Wani, O.M.; Verpaalen, R.; Zeng, H.; Priimagi, A.; Schenning, A.J. An artificial nocturnal flower via humidity-gated photoactuation in liquid crystal networks. *Adv. Mater.* **2019**, *31*, 1805985. [[CrossRef](#)]
37. Hussain, S.; Park, S.Y. Optical glucose biosensor based on photonic interpenetrating polymer network with solid-state cholesteric liquid crystal and cationic polyelectrolyte. *Sens. Actuators B Chem.* **2020**, *316*, 128099. [[CrossRef](#)]
38. Kim, Y.J.; Park, S.Y. Optical Multisensor array with functionalized photonic droplets by an interpenetrating polymer network for human blood analysis. *ACS Appl. Mater. Interfaces* **2020**, *12*, 47342–47354. [[CrossRef](#)]
39. Myung, D.B.; Hussain, S.; Park, S.Y. Photonic calcium and humidity array sensor prepared with reactive cholesteric liquid crystal mesogens. *Sens. Actuators B Chem.* **2019**, *298*, 126894. [[CrossRef](#)]
40. Hussain, S.; Park, S.Y. Sweat-based noninvasive skin-patchable urea biosensors with photonic interpenetrating polymer network films integrated into PDMS chips. *ACS Sens.* **2020**, *5*, 3988–3998. [[CrossRef](#)]
41. Wijayarathna, U.N.; Kiridena, S.D.; Adams, J.D.; Behrend, C.J.; Anker, J.N. Synovial Fluid pH Sensor for Early Detection of Prosthetic Hip Infections. *Adv. Funct. Mater.* **2021**, *31*, 2104124. [[CrossRef](#)]
42. Jang, J.-H.; Park, S.-Y. pH-responsive cholesteric liquid crystal double emulsion droplets prepared by microfluidics. *Sens. Actuators B Chem.* **2017**, *241*, 636–643. [[CrossRef](#)]
43. Noh, K.G.; Park, S.Y. Biosensor array of interpenetrating polymer network with photonic film templated from reactive cholesteric liquid crystal and enzyme-immobilized hydrogel polymer. *Adv. Funct. Mater.* **2018**, *28*, 1707562. [[CrossRef](#)]
44. Jung, S.; Kaar, J.L.; Stoykovich, M.P. Design and functionalization of responsive hydrogels for photonic crystal biosensors. *Mol. Syst. Des. Eng.* **2016**, *1*, 225–241. [[CrossRef](#)]
45. Yoon, S.; Park, H.; Lee, W. Fabrication of inverse opal photonic gel sensors on flexible substrates by transfer process. *Lab Chip* **2021**, *21*, 2997–3003. [[CrossRef](#)]
46. Park, H.; Koh, Y.G.; Lee, W. Smartphone-based colorimetric analysis of structural colors from pH-responsive photonic gel. *Sens. Actuators B Chem.* **2021**, *345*, 130359. [[CrossRef](#)]
47. Cai, Z.; Smith, N.L.; Zhang, J.-T.; Asher, S.A. Two-Dimensional Photonic Crystal Chemical and Biomolecular Sensors. *Anal. Chem.* **2015**, *87*, 5013–5025. [[CrossRef](#)]
48. Ding, H.; Liu, C.; Ye, B.; Fu, F.; Wang, H.; Zhao, Y.; Gu, Z. Free-Standing Photonic Crystal Films with Gradient Structural Colors. *ACS Appl. Mater. Interfaces* **2016**, *8*, 6796–6801. [[CrossRef](#)]
49. Fei, X.; Lu, T.; Ma, J.; Wang, W.; Zhu, S.; Zhang, D. Bioinspired Polymeric Photonic Crystals for High Cycling pH-Sensing Performance. *ACS Appl. Mater. Interfaces* **2016**, *8*, 27091–27098. [[CrossRef](#)]
50. Qin, J.; Dong, B.; Li, X.; Han, J.; Gao, R.; Su, G.; Cao, L.; Wang, W. Fabrication of intelligent photonic crystal hydrogel sensors for selective detection of trace mercury ions in seawater. *J. Mater. Chem. C* **2017**, *5*, 8482–8488. [[CrossRef](#)]
51. Xiao, F.; Sun, Y.; Du, W.; Shi, W.; Wu, Y.; Liao, S.; Wu, Z.; Yu, R. Smart Photonic Crystal Hydrogel Material for Uranyl Ion Monitoring and Removal in Water. *Adv. Funct. Mater.* **2017**, *27*, 1702147. [[CrossRef](#)]